GDCh Research Article Angewandte International Edition Chemie www.angewandte.org

Check for updates

How to cite: *Angew. Chem. Int. Ed.* **2025**, *64*, e202511396
doi.org/10.1002/anie.202511396

MOFs Hot Paper

Twist-Promoted Photoredox Catalysis in Metal-Organic Framework for Defluorination Reactions

Zhiyi Yang, Chao Li, Peiqi Zhang, Jiaxin Lin, Jiayue Tang, Cheng-Yong Su, Teng-Teng Chen,* and Yangjian Quan**

Abstract: The relatively short excited-state lifetime is one main drawback of organic photosensitizers, resulting in their restricted catalytic capability and high catalyst loadings. We herein report the design of a twisted ligand N^9,N^9,N^{10},N^{10}-tetrakis[(1,1′-biphenyl)-4-carboxylic acid]-9,10-anthracene diamine (H_4TCPDA). Its twisted geometry significantly elongates the lifetime of charge-transfer state as substantiated by detailed ultrafast transient absorption (TA) spectroscopic and electrochemical studies. Moreover, its rigid structure benefits the formation of highly crystalline **Y-TCPDA** metal-organic frameworks (MOFs) with excellent stability toward F^- solutions. Therefore, **Y-TCPDA** competently catalyzes chemoselective defluorinative modifications, a challenge remained in MOF catalysis, and olefin reductive cross-coupling with high turnover numbers of up to 9000. Control experiments underscore the protection of organic photocatalytic centers by the MOF platform, while similar organic catalysts are found to be decomposed in a homogeneous catalytic system.

Introduction

Organofluorine compounds have found significant applications in pharmaceuticals, agrochemicals, and functional materials.[1–3] For instance, around 20% of pharmaceutical and 30% of agrochemical molecules involve fluorine motifs. Moreover, Teflon originated from polymerization of tetrafluoroethylene is one of the most widely used chemical-resistant materials. In addition to the direct incorporation of fluorine-containing functional groups (FGs) to target molecules,[4] chemoselective defluorination represents an alternative strategy to construct organofluorine compounds, diversifying their structural and functional complexity.[5,6] One representative protocol involves the defluorinative functionalization of a $-CF_3$ moiety for achieving $-CF_2$(FG) and $-CF(FG)_2$ functionalities.[7,8] However, the inertness of $-CF_3$ group and difficulty in selectivity control restrict its advance. Although several homogeneous catalytic systems have been established,[9–12] engineering a heterogenous catalyst for $-CF_3$ defluorinative functionalization remains elusive.[13]

Organic photosensitizers (PSs) have emerged as promising alternatives to noble-metal-based photosensitizers, featuring relatively low costs, wide accessibility, good catalytic performance, and sustainable/environmentally benign nature. For example, they prove effective in defluorination transformations, attributing to their matched redox properties upon excitation.[14–16] Despite fruitful achievements, challenges still remain regarding the relatively short excited-state lifetime and poor stability of organic PSs.[17] Consequently, relatively high catalyst loadings are often required in homogeneous catalytic systems.[18]

We hypothesized that a rationally designed metal-organic framework (MOF) catalyst would provide a solution to the above challenges.[19–28] On the one hand, their good tunability and unique porous structure make MOFs a good platform for engineering heterogeneous catalysis.[29–39] On the other hand, MOFs have demonstrated their superior ability in protecting active catalytic centers from catalyst poisoning.[40–45] However, to the best of our knowledge, MOF-catalyzed chemoselective defluorinative functionalization remains relatively underdeveloped,[46–49] in comparison to other organic transformations.[50–55] To achieve this goal, several factors need to be concerned. First, the MOF catalyst should be stable enough under defluorinative reaction conditions, which is challenging to obtain for most MOFs (vide infra).[56–61] Second, the MOFs are expected to possess wide pores or channels for accommodating complex reagents. Third, the heterogenization by MOFs would not significantly change the photophysical properties of organic PSs.

Taking the above design criteria into consideration, N^1,N^1,N^4,N^4-[(1,1′-biphenyl)-4-carboxylic acid]-1,4-benzene diamine (H_4TPBD) was initially evaluated as a PS, however, with poor activity (entry 1, Table S3 in Supporting Information). The short lifetime of 115 ps for the charge-transfer state of H_4TPBD accounts for the inferior performance (Figure 2k, vide infra). To elongate the

[*] Z. Yang, Dr. C. Li, P. Zhang, J. Lin, J. Tang, Prof. Dr. T.-T. Chen, Prof. Dr. Y. Quan
Department of Chemistry, The Hong Kong University of Science and Technology, Clear Water Bay, Hong Kong, China
E-mail: tengtengchen@ust.hk
chyjquan@ust.hk

Prof. Dr. C.-Y. Su
GBRCE for Functional Molecular Engineering, MOE Laboratory of Bioinorganic and Synthetic Chemistry, LIFM, IGCME, School of Chemistry, Sun Yat-Sen University, Guangzhou, China
E-mail: cesscy@mail.sysu.edu.cn

Additional supporting information can be found online in the Supporting Information section

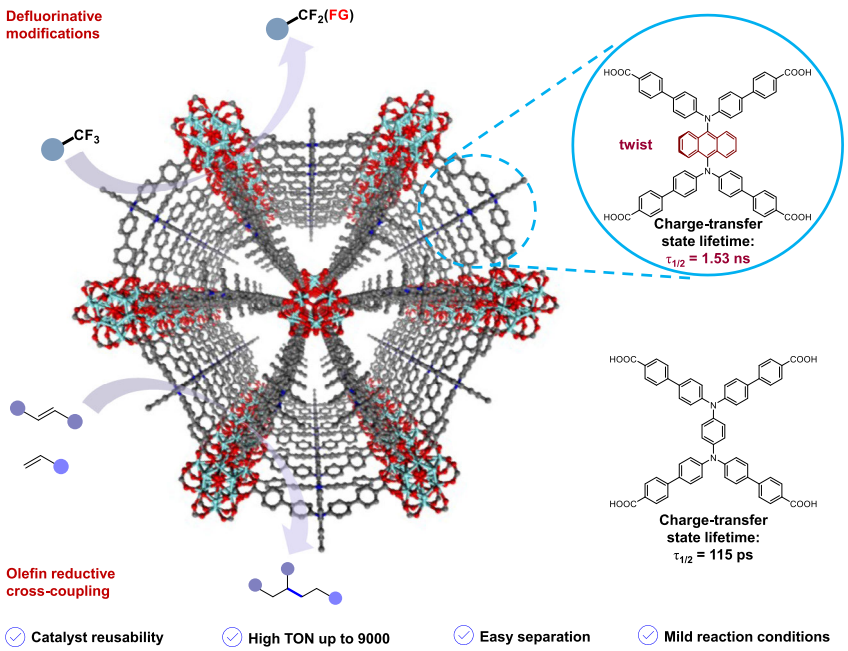

Figure 1. **Y-TCPDA** MOFs bridged by a twisted photocatalytic ligand for sustainable photoredox catalysis, TON = turnover numbers.

excited-state lifetime, N^9,N^9,N^{10},N^{10}-tetrakis[(1,1′-biphenyl)-4-carboxylic acid]-9,10-anthracene diamine (H_4TCPDA) was subsequently designed and newly prepared (Figure 1). Its twisted geometry was conceived to retard charge recombination of the excited state and therefore result in a longer lifetime (1.63 ns, Figure 2k, vide infra).

After many attempts, highly crystalline MOF **Y-TCPDA**, consisting of Y_9-building units and H_4TCPDA linkers, has been prepared. It effectively catalyzed $-CF_3$ defluorinative derivatization and olefin reductive cross-coupling with turnover numbers (TON) of up to 9000. Its superior catalytic performance is attributed to the relatively long excited-state lifetime (1.53 ns, Figure 2k, vide infra) and excellent stability toward F^- solutions. Ultrafast transient absorption (TA) spectroscopic and electrochemical studies substantiate the long charge-transfer state of **Y-TCPDA**. Moreover, detailed control experiments evidence the protection of organic PSs by the MOF platform. In contrast, the Me_4TCPDA catalytic center is subjected to decay and degradation under homogeneous catalytic conditions.

Results and Discussion

H_4TPBD has been reported and utilized as an organic linker to prepare different types of MOFs.[62,63] Good flexibility in the orientation of four carboxylic binding sites of H_4TPBD leads to various structures of generated MOFs. In sharp contrast, our newly prepared H_4TCPDA, which incorporates an anthracene moiety in place of the middle benzene motif in H_4TPBD, was anticipated to be more rigid,[38] thus improving the stability of generated MOFs. As evidenced by the single crystal structure of H_4TCPDA (Figure 2a), the four carboxylic binding sites are almost in the same plane, perpendicular to the anthracene motif. Such a twisted structure is also expected to prolong the charge-transfer lifetime (τ) of the excited state.[64]

Treatment of H_4TCPDA, $Y(NO_3)_3{\cdot}6H_2O$, and modulator 2-fluorobenzoic acid (2-FBA) in *N,N*-dimethylformamide (DMF) at 120 °C for 48 h yielded prism yellow crystals of **Y-TCPDA** (Figure 2a). Single crystal X-ray diffraction (SC-XRD) indicated a space group of *P6* (No. 189) with a, b = 48.4 Å and c = 17.9 Å for **Y-TCPDA**.[65,66] It consists of 12-connected Y_9 clusters bridged by TCPDA linkers, wherein the TCPDA unit remained the twisted structure. The highly crystalline structure of **Y-TCPDA** was further proved by powder X-ray diffraction (PXRD) analyses (Figure 2c). Scanning electron microscope (SEM) imaging demonstrated the hexagonal prism morphology of **Y-TCPDA** (Figure 2d).

The structure and composition of **Y-TCPDA** were further verified by NMR spectroscopy, thermogravimetric analysis (TGA), energy dispersive spectroscopy (EDS) elemental mapping, and X-ray photoelectron spectroscopy (XPS). The ^{1}H NMR spectrum of digested **Y-TCPDA** showed one set of signals assignable to the H_4TCPDA ligand (Figure 2e). Meanwhile, the ^{19}F NMR spectrum of digested **Y-TCPDA** indicated the involvement of HF, probably originating from Y-F moieties in **Y-TCPDA**. To verify this possibility, XPS was conducted. The peak at 685.2 eV was assigned to the metal fluoride species (Figure S18 in Supporting Information).[67] Moreover, EDS elemental mapping suggested that Y, C, N, O, and F are evenly distributed in **Y-TCPDA** (Figure S16 in Supporting Information). According to the above characterizations, a plausible chemical formula of $\{DMA_1[Y_9(\mu_3\text{-}O)_2(\mu_3\text{-}OH)_{6.7}(\mu_3\text{-}F)_{5.3}(TCPDA)_3]{\cdot}(solv)_x\}$ (DMA = dimethylammonium cation, solv = solvent) was

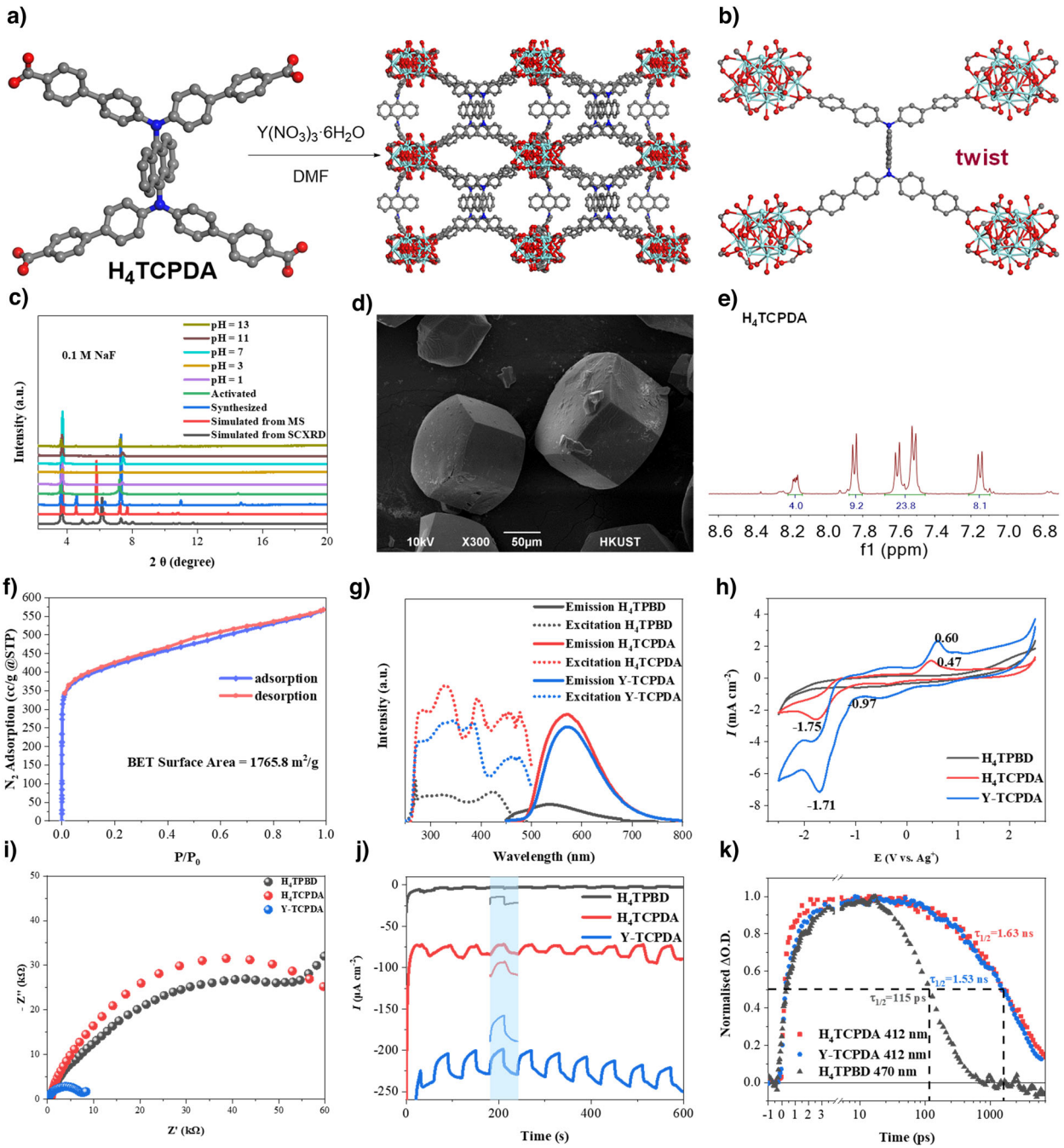

Figure 2. a) Schematic showing the synthesis of **Y-TCPDA** and the structure: single crystal structure viewed from a axis; some disorder and H atoms are omitted for clarity; light blue: Y, red: O, blue: N, and gray: C. b) Diagram of H_4TCPDA coordinated with Y_9-SBUs, showing its twisted structure. c) PXRD patterns of **Y-TCPDA** after being soaked in 0.1 M NaF aqueous solutions with different pH from 1 to 13, MS = Materials Studio, SCXRD = single crystal X-ray Diffraction. d) Scanning electron microscopy of **Y-TCPDA**. e) Zoom-in ^{1}H NMR of digested **Y-TCPDA** in DMSO-d_6. f) N_2 (77 K) adsorption and desorption isotherms for the activated **Y-TCPDA**, BET = Brunauer–Emmett–Teller. g) Excitation and emission spectra of H_4TPBD, H_4TCPDA, and **Y-TCPDA**. h) Cyclic voltammetry spectra of H_4TPBD, H_4TCPDA, and **Y-TCPDA** in MeCN. i) Electrochemical impedance spectroscopy of H_4TPBD, H_4TCPDA, and **Y-TCPDA** in MeCN. j) Transient photocurrent of H_4TPBD, H_4TCPDA, and **Y-TCPDA** upon irradiation by a Kessil PR160L-390 lamp. k) Normalized kinetic traces of excited-states of H_4TCPDA, **Y-TCPDA**, and H_4TPBD excited at 390 nm and probed at 412, 412, and 470 nm, respectively. The dashed line indicates the corresponding timescale when the optical density decreased by 50%; ΔO.D. = difference in optical density.

proposed for **Y-TCPDA**. The formula was then substantiated by TGA. The experimental weight loss of 71.0% is consistent with a calculated weight loss of 75.0% for the conversion of $\{DMA_1[Y_9(\mu_3\text{-}O)_2(\mu_3\text{-}OH)_{6.7}(\mu_3\text{-}F)_{5.3}(TCPDA)_3]\}$ to $(Y_2O_3)_{4.5}$.

Y-TCPDA exhibited considerable thermal stability upon heating up to 500 °C. Furthermore, it retained the crystalline structure after being soaked in 0.1 M aqueous solution of NaF across a wide pH range (from 1 to 13) and in various polar solvents (Figures 2c and S31 in Supporting Information), suggesting its excellent stability toward F^- under basic or acidic conditions. The porosity of **Y-TCPDA** was investigated through gas absorption analyses. The Brunauer–Emmett–Teller surface area was measured as 1765.8 $m^2\ g^{-1}$ with main pore size of 13.0 Å (Figures 2f and S12 in Supporting Information). After being soaked in 0.1 M NaF aqueous solution, **Y-TCPDA** exhibited surface areas of 1609.0 $m^2\ g^{-1}$ (pH = 1) and 1141.1 $m^2\ g^{-1}$ (pH = 13), respectively (Figure S36–S37), further demonstrating its good chemical stability.

Y-TCPDA and H_4TCPDA exhibited similar emission and excitation properties (Figure 2g). The stronger emission intensity of **Y-TCPDA** and H_4TCPDA compared with H_4TPBD may be attributed to the increased charge separation in **Y-TCPDA** and H_4TCPDA. Moreover, upon excitation, the excited-state lifetime ($\tau_{1/2}$) of **Y-TCPDA**, H_4TCPDA, and H_4TPBD was measured as 1.53, 1.63, and 115 ps, respectively (Figure 2k). **Y-TCPDA** and H_4TCPDA possess about 15 times longer lifetimes of the charge-transfer state (Figure 4g–i, see detailed TA studies vide infra) compared to H_4TPBD, implying their superior photocatalytic performance.

Cyclic voltammetry (CV) experiments indicated the redox potential of **Y-TCPDA** (−1.71/0.60 V vs. Ag^+), H_4TCPDA (−1.75/0.47 V vs. Ag^+), and H_4TPBD (−0.97/0.85 V vs. Ag^+), respectively (Figure 2h). Upon combining with the luminescence profile, the redox potential of excited **Y-TCPDA** was accordingly calculated as 0.48/−1.59 V vs. Ag^+. **Y-TCPDA** exhibited a decreased recombination resistance in electrochemical impedance spectroscopy (EIS) compared to H_4TCPDA and H_4TPBD (Figure 2i). Transient photocurrent responses of **Y-TCPDA** also demonstrated higher photocurrents than those of H_4TCPDA and H_4TPBD (Figure 2j). Furthermore, the photocurrent curve of H_4TPBD was found to be relatively sharp.

Chemoselective defluorinative functionalization has proven to be an effective strategy to diversify the structural and functional complexity of organofluorine compounds. Its side product is F^-, which often cannot be tolerated by many MOFs. Therefore, little precedents regarding MOF-catalyzed chemoselective defluorinative modification have hitherto been reported.[56] Given the excellent stability of **Y-TCPDA** toward F^- and its matched photophysical properties, **Y-TCPDA** was initially evaluated as a heterogeneous PS for $-CF_3$ defluorination. In the presence of **Y-TCPDA** (1 mol% based on the linker) and sodium formate, treatment of **1a** in DMSO under light irradiation afforded the target **2a** in 95% yield. Noteworthily, no external hydrogen atom transfer (HAT) cocatalyst was required in our MOF catalytic system, because it in-situ generated thiol catalyst from dimethyl sulfoxide (DMSO) (vide infra). Contrastingly, homogeneous catalytic systems necessitate the thiol (5–20 mol%) as the HAT cocatalyst (Figure S39 in Supporting Information).

We then explored the scope of **Y-TCPDA** catalyzed defluorination (Figure 3a). Different substituents on the phenyl ring were tolerated, including fluoride, chloride, trifluoromethoxy, ether, and alkyl groups (**2a**–**2h**, **2l**, **2m**). However, if the substrate contained bromo or iodo groups, debromination or deiodination occurred in company with the target defluorination (**2i**). Pyridine-bearing substrates worked well to afford **2j** and **2k** in ≥70% yields. Notably, the defluorination degree could be controlled by tuning the reaction time. Elongating the time from 12 h to 24 h, the didefluorination product **2n-2** was obtained as the main product. Moreover, by slightly modifying reaction conditions, the per-defluorination product **2n-3** was isolated in 53% yield.

To our delight, **Y-TCPDA** effectively catalyzed defluorination of trifluorotoluene (**2o**), which features a notably high reduction potential of −3.04 V versus Fc^+/Fc in acetonitrile (MeCN) and is hard to undergo defluorination under photocatalytic conditions. To the best of our knowledge, a very limited number of photocatalytic systems have been developed, which require the assistance of heating to 100 °C or stoichiometric amounts of boron reagents (Figure S39 in SI).[7,11,68] Notably, this MOF catalytic system was successfully applied to the reductive defluorination of other trifluoromethyl aromatics (**2p–2r**).

In addition to defluorination, defluorinative alkylation was also tested by using the **Y-TCPDA** catalyst. A series of trifluoromethyl amides and esters reacted with 1-octene smoothly to give **3a**–**3l**. Just like the above defluorination, the mono- and di-alkylation could be selectively obtained by controlling the reaction time (**3j** and **3k**). Other olefins including acyl or hydroxyl groups, cyclooctene, and diolefins were also compatible (**3m**–**3s**). Meanwhile, a collection of unactivated trifluoromethyl aromatics were engaged in defluorinative alkylation, affording the desired products **3t**–**3y** in good yields.

In view of the good reducing ability of **Y-TCPDA**, its catalytic capability in facilitating reductive cross-coupling of alkenes was explored. In the presence of **Y-TCPDA** (0.5 mol%), thiol (20 mol%, HAT cocatalyst), and γ-terpinene (1.0 equiv, hydrogen donor), treatment of dimethyl maleate with styrene in 1,2-dichloroethane (DCE) at room temperature under light irradiation for 24 h yielded the desired cross-coupling products. Different functional groups involving bromide, chloride, fluoride, alkyl, methoxy, and amino on the phenyl ring were tolerated (**4a**-**4i**). Alkyl olefins also served as good coupling partners, and the corresponding **4j**–**4l** were obtained in moderate yields. Additionally, reductive coupling between styrene and cyclic *N*-methylmaleimide proceeded smoothly to afford **4m**.

Derivatives of bioactive and drug molecules, such as menthol, borneol, and estrone, were compatible with **Y-TCPDA** catalysis (**2s**, **3z**-**3ab**). The molecular size of product **3ab** is up to 16.9 Å, indicating the good accommodation of **Y-TCPDA** catalysis toward large molecules.

The use of Me_4TCPDA (1 mol%) as a homogeneous catalyst led to **2a** in 67% yield (entry 2, Table S3). However, after reaction, the Me_4TCPDA catalyst disappeared according to

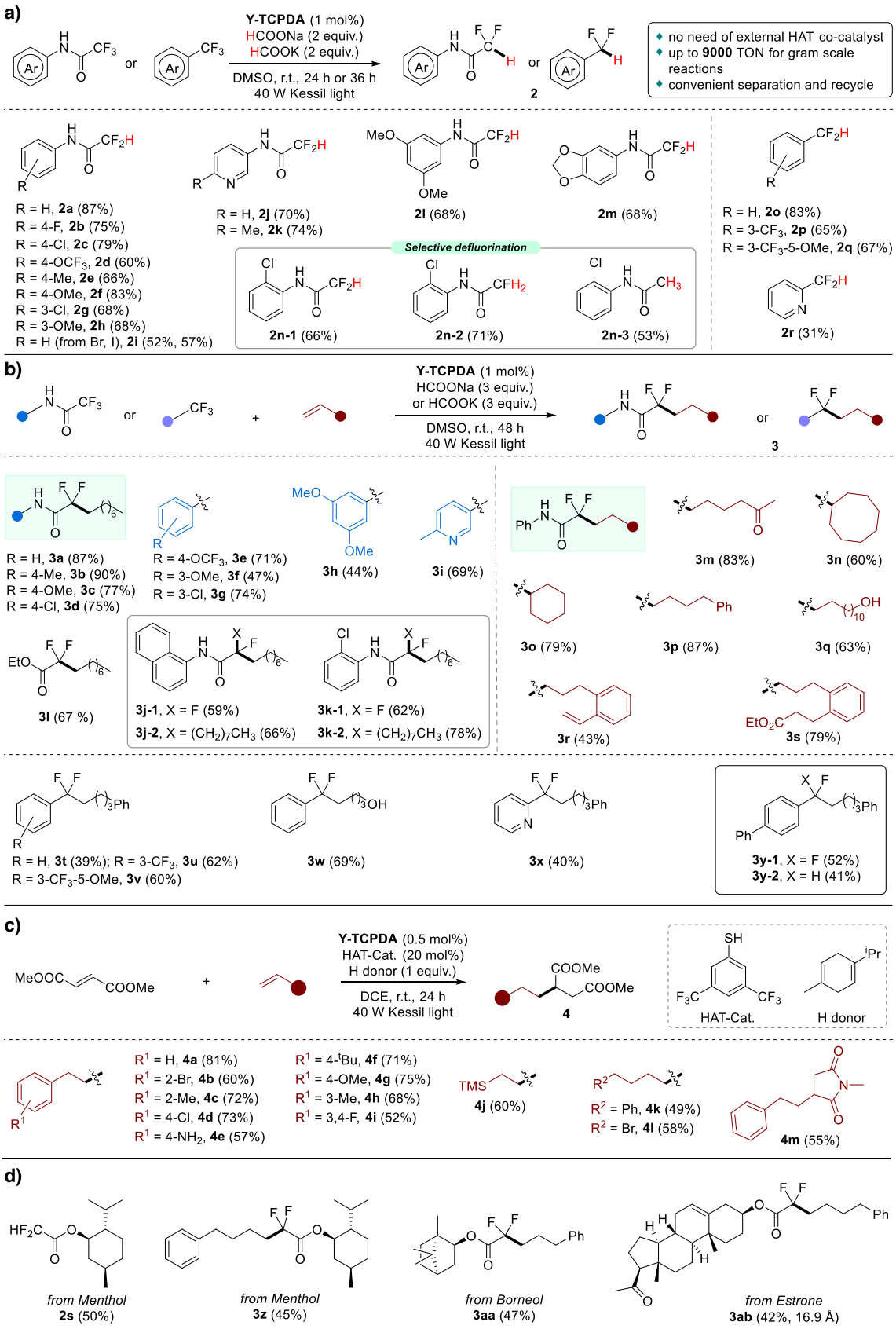

Figure 3. **Y-TCPDA** catalyzed chemoselective defluorination a), defluorinative alkylation b), olefin reductive cross-coupling c), and defluorinative transformations of bioactive molecule derivatives d).

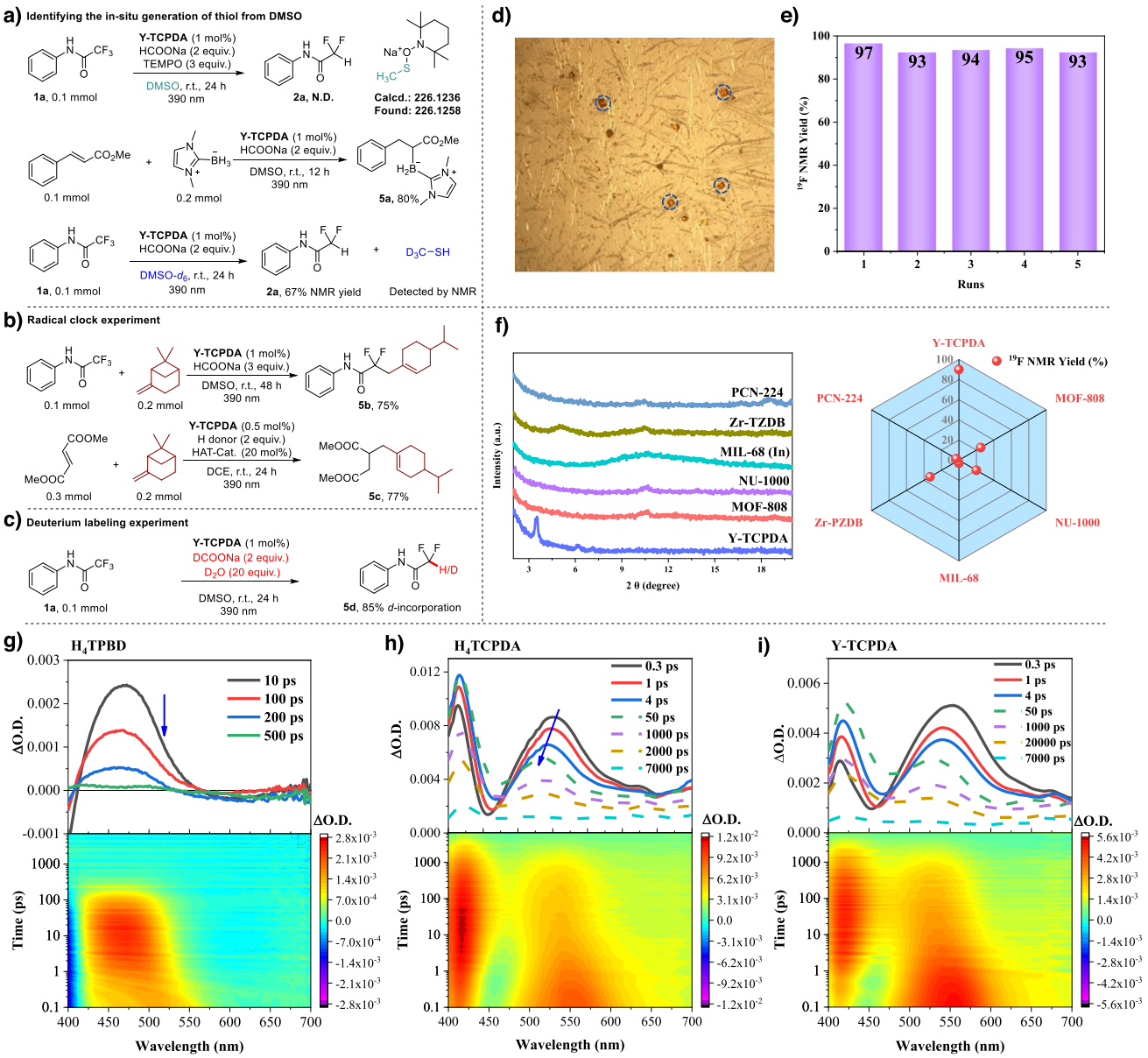

Figure 4. Mechanistic investigations. a) Experiments to illustrate the in-situ generation of CH_3SH from DMSO. b) Radical clock experiments. c) Deuterium labeling experiment. d) Figure of **Y-TCPDA** crystals (in blue cycle) after reaction. e) Recycle test, yields of **2a** in 5 runs. f) Employment of other MOFs as the catalyst for defluorination and their stability evaluation after the reaction. g)–i) Transient absorption spectra of H_4TPBD g), H_4TCPDA h), and **Y-TCPDA** i) at selected pump-probe time delays, and the corresponding complete transient absorption surface probed; ΔO.D. = difference in optical density; all TA spectra were recorded in DMSO following 390 nm excitation.

^{1}H NMR, TLC, and HRMS analyses (Figures S71–S74 in Supporting Information), suggesting its susceptibility under standard reaction conditions. Conversely, **Y-TCPDA** catalyst retained its crystalline structure after reaction as evidenced by PXRD and microscope analyses (Figures 4d,f and S32–S35 in Supporting Information). In addition, ^{1}H NMR spectrum of recovered **Y-TCPDA** showed identical peaks assignable to H_4TCPDA ligand (Figure S75 in Supporting Information), highlighting the protection of the organic PSs by the MOF platform.[59] In view of the robustness of **Y-TCPDA**, an experiment with an extra low catalyst loading of 0.01 mol% was performed. The target **2a** was obtained in 90% yield after 48 h irradiation, leading to a TON of 9000 (entry 5, Table S3). No reaction was detected in the absence of **Y-TCPDA** or in the dark (entries 8 and 10, Table S3). Notably, the **Y-TCPDA** catalyst could be easily recovered and reused as the catalyst for at least five runs without obvious decay in the catalytic performance (Figures 4e and S68–S70 in Supporting Information). Other MOFs as the catalyst provided inferior efficiencies (Figure 4f, right), due probably to their susceptibility under defluorinative reaction conditions (Figure 4f, left).[56–61]

To elucidate the excited electronic states and photocatalytic mechanisms of **Y-TCPDA**, ultrafast TA spectroscopic

studies were performed (Figure 4g–i). First, TA spectra of H_4TCPDA showed a broad photoinduced absorption (PIA) peak across the visible region between 470 and 700 nm (Figure 4h, ~555 nm at 0.3 ps) and a sharp and intense peak at ~412 nm upon excitation. Introducing 2-methyl-2-propanethiol and sodium formate as the electron donor extended the lifetime of the ~555 nm spectral feature (Figure S43), while oxygen as the electron acceptor quenched this signal and prolonged the PIA at ~412 nm (Figures S44). These results indicate that the broad PIA (~555 nm) and the sharp one (~412 nm) correspond to the reduced and oxidized H_4TCPDA charge-transfer (CT) states, respectively. The bands between 470 and 700 nm in the TA spectra of H_4TCPDA were blue shifted from ~555 to ~535 nm over the first 50 ps. This blue shifting is commonly observed in some donor-acceptor molecules, suggesting the high freedom of molecular rotation combined with solvent reorganization and vibrational cooling.[69,70,71]

In contrast, the TA spectra of unmodified H_4TPBD displayed only one PIA band centered at 470 nm, overlapping with the negative ground-state bleach (GSB) (Figure 4g), which decayed rapidly with $t_{50\%}$ (the time for the maximum PIA to decay by 50%) at ~115 ps. In comparison, H_4TCPDA exhibited significantly prolonged excited states ($t_{50\%} \approx 1.63$ ns), suggesting that the structural modification of H_4TPBD into H_4TCPDA can enhance photogenerated charge carrier lifetime and charge transport efficiency, supporting the superior photocatalytic activity of H_4TCPDA over H_4TPBD.

The TA spectra of Y-TCPDA in DMSO following 390 nm excitation closely resembled those of H_4TCPDA, with broader PIAs tentatively attributed to excitonic delocalization through intermolecular interactions facilitated by the MOF structure. The more ordered crystalline framework of Y-TCPDA improved charge mobility, enabling efficient transport of photogenerated charge carriers to catalytic sites.

Decay trace fitting for radical anionic H_4TCPDA and **Y-TCPDA** revealed three exponential components, for H_4TCPDA ($\tau_1 = 1.2 \pm 0.1$ ps, $\tau_2 = 12 \pm 1$ ps, and $\tau_3 = 2.3 \pm 0.1$ ns at 555 nm; $\tau_1 = 1.4 \pm 0.1$ ps, $\tau_2 = 18 \pm 2$ ps, and $\tau_3 = 2.3 \pm 0.05$ ns at 535 nm) and for **Y-TCPDA** ($\tau_1 = 2.1 \pm 0.1$ ps, $\tau_2 = 41 \pm 5$ ps, and $\tau_3 = 2.2 \pm 0.1$ ns at 555 nm; $\tau_1 = 2.2 \pm 0.1$ ps, $\tau_2 = 64 \pm 8$ ps, and $\tau_3 = 2.4 \pm 0.1$ ns at 535 nm), permitting the comparison of the lifetimes at different stages (Figures S45, S46). The initial component τ_1 (1.2–2.2 ps) represents the rapid local excited (LE) or charge transfer (CT) states formation in both H_4TCPDA and **Y-TCPDA**. The subsequent process τ_2 (12–64 ps) is associated with molecular conformational changes, and the last process τ_3 (~2.2 ns) represents relaxed CT states. **Y-TCPDA** displayed relatively longer τ_1, τ_2, and similar τ_3 lifetimes compared with H_4TCPDA. These results imply the role of MOF structures in extending charge transport lifetimes and enhancing catalytic efficiency.

In the homogeneous catalytic systems,[14,72] both PS and HAT cocatalyst are required for achieving defluorination and defluorinative alkylation. In contrast, our **Y-TCPDA** catalysis does not involve the addition of a HAT cocatalyst. To get some insights into this unique phenomenon, several control experiments were conducted. The addition of a radical capture 2,2,6,6-tetramethylpiperidinooxy (TEMPO) to the reaction effectively inhibited the formation of **2a** but afforded a thiol radical capture product, suggesting the in-situ generation of the $CH_3S^{\cdot}$ species from the solvent DMSO (Figure 4a). In addition, our **Y-TCPDA** catalysis competently enabled the hydroboration of methyl cinnamate with *N*-heterocyclic carbene (NHC) borane, which was reportedly facilitated by a thiol radical catalyst.[73] More importantly, the use of DMSO-d_6 as the solvent permitted the detection of CD_3SH, providing a solid evidence for in-situ formation of methanethiol from DMSO (Figures 4a and S51 in Supporting Information). In view of these experimental observations and according to literature precedents,[74] a plausible mechanism for generating the thiol radical from DMSO though **Y-TCPDA** photoactivation was proposed in Figure 5a. Further ^{1}H NMR analyses suggested the formation of NaOMe side product (Figures S49, S50 in Supporting Information), supporting the proposed pathway for $CH_3S^{\cdot}$ formation.

The addition of bicyclic terpene β-pinene, a radical clock reagent, resulted in the ring-opening products (**5b** and **5c**), underscoring the involvement of related radical species in defluorinative modifications and olefin reductive cross-coupling (Figure 4b). A series of deuterium labelling experiments were carried out (Figures 4c and S76–S83 in Supporting Information). Employment of DCOONa instead of HCOONa, accompanied with the addition of D_2O, led to an 85% deuterium incorporation in **5d**, while using these deuterium sources individually provided only 60% and 57% deuteration ratios, respectively. These results suggested that the hydrogen in the defluorination products might originate from sodium formate and proton in DMSO. The same conclusion was obtained in defluorinative alkylation according to the corresponding deuterium labeling experiments (Table S6). The addition of D_2O to the reaction of dimethyl fumarate with styrene led to deuteration of three C─H moieties in **5f** with 32%–44% incorporation ratios (Figures S108, S109 in Supporting Information).

Quenching experiments using Me_4TCPDA as the PS were conducted to shed light on the reaction mechanisms. Notably, 2-methyl-2-propanethiol was used instead of MeSH, because the latter is a gas and difficult to handle. As shown in Figure S56, only a combination of the thiol and HCOONa could quench the excited Me_4TCPDA effectively with a K_{sv} of 0.0014 for the corresponding Stern–Volmer curve. For olefin reductive cross-coupling, the excited PS could be quenched by dimethyl fumarate not styrene, with a K_{sv} of 0.0072 (Figures S58–S60 in Supporting Information).

The results of light on/off experiments for three model reactions suggested that defluorination and olefin reductive coupling did not involve a radical chain mechanism, while defluorinative alkylation might partially undergo a radical chain pathway (Figures S61–S66 in Supporting Information). The corresponding quantum yields for these model reactions were measured as 0.22, 0.65, and 0.07, respectively (see Section 5.7 in Supporting Information), in line with the above observations regarding the radical chain pathway. Hot filtration experiments were subsequently performed. No obvious yield improvement was observed after removing the

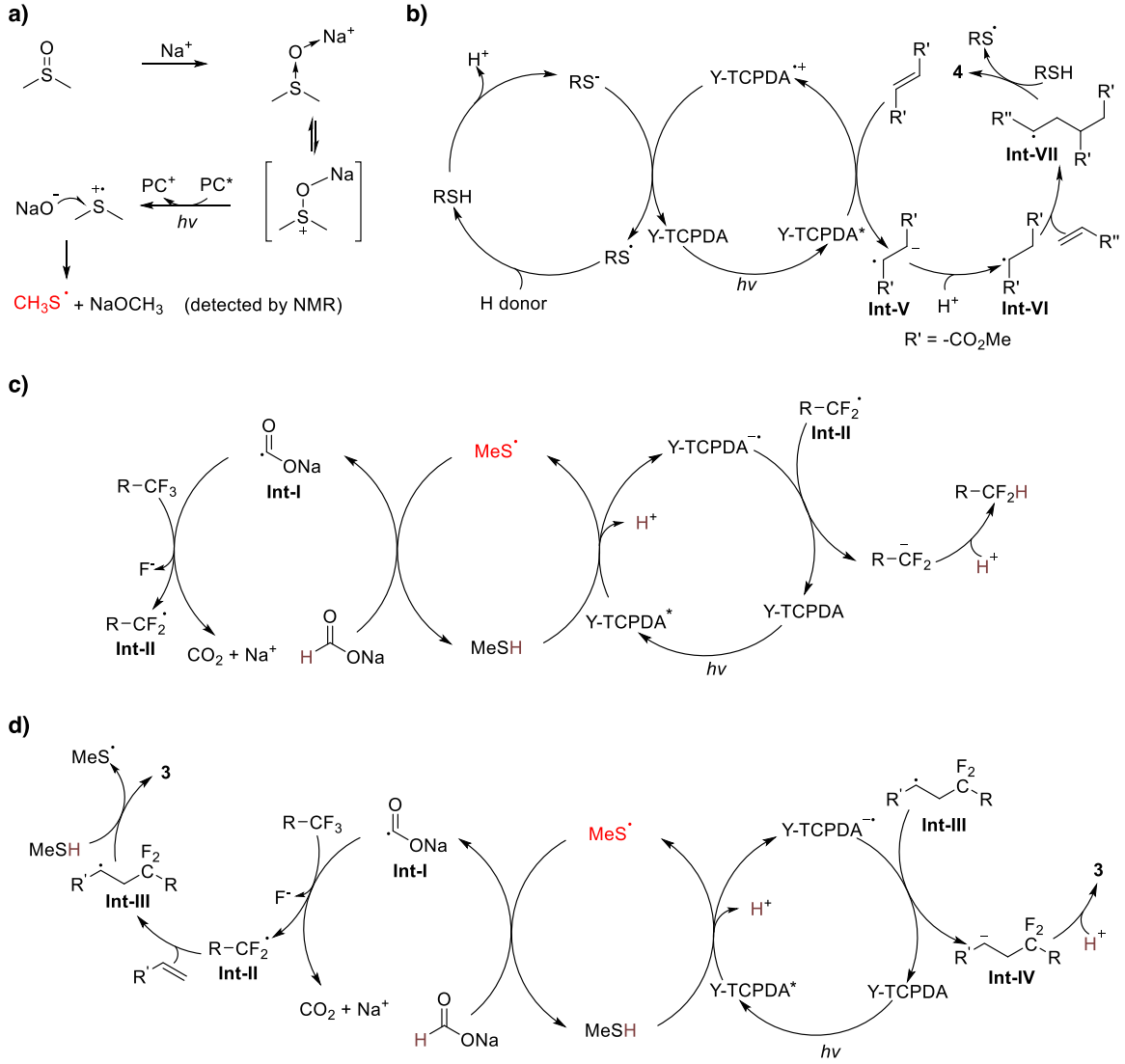

Figure 5. Proposed mechanisms for the in-situ generation of thiol radical a), olefin reductive cross-coupling b), defluorination c), and defluorinative alkylation d).

MOF catalyst for defluorination and olefin reductive coupling (see Section 5.8 in Supporting Information). However, the model reaction of defluorinative alkylation continued after the removal of MOF catalyst, resulting in a yield increase from 51% to 63% for **3a**, due probably to its partial radical chain pathway. These experimental observations also substantiate the heterogeneous nature of this **Y-TCPDA** catalysis.

Based on the above experimental observations and literature precedents,[14,75] plausible reaction mechanisms were proposed in Figure 5 for three model reactions. First, our MOF catalytic system generates MeS˙ from DMSO upon light irradiation (Figure 5a). The thiol radical then undergoes HAT with HCOONa to give the carbon dioxide radical anion (**Int-I**), which is highly reactive to reduce the substrate R-CF_3. The resulting RCF_2˙ (**Int-II**) is further reduced by the excited **Y-TCPDA**, followed by protonation to yield the defluorination product **2** (Figure 5c). Alternatively, the RCF_2˙ radical attacks an olefin to form a carbon radical intermediate (**Int-III**), which is then subjected to HAT with the thiol or a sequence of reduction and protonation to deliver defluorinative alkylation product **3** (Figure 5d). For olefin reductive cross-coupling, the dimethyl fumarate is first reduced by the excited **Y-TCPDA** to become a radical anion (**Int-V**), which undergoes protonation and then attacks an olefin to give a new carbon radical intermediate (**Int-VII**) (Figure 5b). This intermediate undergoes HAT with the thiol to afford the cross-coupling product.

Conclusion

In summary, we have designed and synthesized a structurally twisted ligand H_4TCPDA. Its twisted geometry not only facilitates the synthesis of hexagonal prism MOF **Y-TCPDA**, but also results in a significantly elongated lifetime of the charge-transfer state of excited **Y-TCPDA**. The excellent

stability and relatively long excited-state lifetime of **Y-TCPDA** contribute to the first realization of chemoselective defluorinative modifications in MOF catalysis. In addition, **Y-TCPDA** effectively catalyzes the reductive cross-coupling of olefins. Several bioactive molecules with sizes of up to 16.9 Å are also compatible with **Y-TCPDA** catalysis.

The homogeneous control experiment implies the decay of organic PS under the defluorinative reaction conditions. Conversely, our MOF platform has proved effective in protecting the catalytic center with high TONs of up to 9000 and remarkable recyclability. Furthermore, our **Y-TCPDA** catalytic system can in-situ generate $CH_3S^{\cdot}$ co-catalyst from DMSO and therefore avoid the need of external HAT co-catalyst (5–20 mol%), essential in previously developed catalysis. This research underscores the potential of rational ligand design in MOF synthesis and applications, providing a useful reference to photocatalysis with organic PSs.

Acknowledgements

The authors acknowledge the start-up fund (R9804 to Y.Q., R9874 to T.T.C.) from HKUST, Early Career Scheme from the Research Grants Council of Hong Kong (26307123 to Y.Q., 26311224 to T.T.C.), NSFC Young Scholar Fund (22301254 to Y.Q.), the NSFC/RGC Joint Scheme (N_HKUST613/24 to Y.Q.), the YCRF from the Research Grants Council of Hong Kong (C7001-23Y to Y.Q.), the Young Elite Scientists Sponsorship Program by the China Association for Science and Technology (CAST) (2023QNRC001 to T.T.C.), and open research fund of Key Laboratory of Precision and Intelligent Chemistry. Dr. Herman Ho-Yung SUNG and Prof. Dr. Ian Williams are acknowledged for X-ray crystallography. The authors thank Prof. Dr. Haipeng LU for sharing instruments.

Conflict of Interests

The authors declare no conflict of interest.

Data Availability Statement

The data that support the findings of this study are available in the Supporting Information of this article. CCDC 2411176 (for H4TCPDA) and 2448299 (for Y-TCPDA) contain the supplementary crystallographic data for this paper. These data can be obtained free of charge from Cambridge Crystallographic Data Centre https://www.ccdc.cam.ac.uk/structures/.

Keywords: Heterogeneous catalysis · Hybrid materials · MOF · Photocatalysis · Twisted photosensitizer

[1] R. Berger, G. Resnati, P. Metrangolo, E. Weber, J. Hulliger, *Chem. Soc. Rev.* **2011**, *40*, 3496.
[2] Y. Zhou, J. Wang, Z. N. Gu, S. N. Wang, W. Zhu, J. L. Aceña, V. A. Soloshonok, K. Izawa, H. Liu, *Chem. Rev.* **2016**, *116*, 422–518.
[3] N. A. Meanwell, *J. Med. Chem.* **2018**, *61*, 5822–5880.
[4] J. A. Ma, D. Cahard, *Chem. Rev.* **2004**, *104*, 6119–6146.
[5] X. Y. Yang, T. Wu, R. J. Phipps, F. D. Toste, *Chem. Rev.* **2015**, *115*, 826–870.
[6] C. F. Ni, J. B. Hu, *Chem. Soc. Rev.* **2016**, *45*, 5441–5454.
[7] D. B. Vogt, C. P. Seath, H. B. Wang, N. T. Jui, *J. Am. Chem. Soc.* **2019**, *141*, 13203–13211.
[8] Y. J. Yu, F. L. Zhang, T. Y. Peng, C. L. Wang, J. Cheng, C. Chen, K. N. Houk, Y. F. Wang, *Science* **2021**, *371*, 1232–1240.
[9] K. Chen, N. Berg, R. Gschwind, B. König, *J. Am. Chem. Soc.* **2017**, *139*, 18444–18447.
[10] C. S. Luo, J. S. Bandar, *J. Am. Chem. Soc.* **2019**, *141*, 14120–14125.
[11] J. Koo, W. Kim, B. H. Jhun, S. Park, D. Song, Y. You, H. G. Lee, *J. Am. Chem. Soc.* **2024**, *146*, 22874–22880.
[12] J. Huang, Q. Gao, T. Zhong, S. Chen, W. Lin, J. Han, J. Xie, *Nat. Commun.* **2023**, *14*, 8292.
[13] T. Ahrens, J. Kohlmann, M. Ahrens, T. Braun, *Chem. Rev.* **2015**, *115*, 931–972.
[14] J. H. Ye, P. Bellotti, C. Heusel, F. Glorius, *Angew. Chem. Int. Ed.* **2022**, *61*, e202115456.
[15] S. S. Yan, S. H. Liu, L. Chen, Z. Y. Bo, K. Jing, T. Y. Gao, B. Yu, Y. Lan, S. P. Luo, D. G. Yu, *Chem* **2021**, *7*, 3099–3113.
[16] M. W. Campbell, V. C. Polites, S. Patel, J. E. Lipson, J. Majhi, G. A. Molander, *J. Am. Chem. Soc.* **2021**, *143*, 19648–19654.
[17] Y. Y. Wu, D. Kim, T. S. Teets, *Synlett* **2022**, *33*, 1154–1179.
[18] N. A. Romero, D. A. Nicewicz, *Chem. Rev.* **2016**, *116*, 10075–10166.
[19] J. R. Long, O. M. Yaghi, *Chem. Soc. Rev.* **2009**, *38*, 1213.
[20] Y. Kim, T. Yang, G. Yun, M. B. Ghasemian, J. Koo, E. Lee, S. J. Cho, K. Kim, *Angew. Chem. Int. Ed.* **2015**, *54*, 13273–13278.
[21] I. Nath, J. Chakraborty, F. Verpoort, *Chem. Soc. Rev.* **2016**, *45*, 4127–4170.
[22] Z. G. Hu, Y. X. Wang, D. Zhao, *Chem. Soc. Rev.* **2021**, *50*, 4629–4683.
[23] M. Zhao, S. Ou, C. D. Wu, *Accounts. Chem. Res.* **2014**, *47*, 1199–1207.
[24] A. M. Shultz, O. K. Farha, J. T. Hupp, S. T. Nguyen, *J. Am. Chem. Soc.* **2009**, *131*, 4204–4205.
[25] J. Liu, T. A. Goetjen, Q. I. Wang, J. G. Knapp, M. C. Wasson, Y. Yang, Z. H. Syed, M. Delferro, J. M. Notestein, O. K. Farha, J. T. Hupp, *Chem. Soc. Rev.* **2022**, *51*, 1045–1097.
[26] Y. B. Huang, J. Liang, X. S. Wang, R. Cao, *Chem. Soc. Rev.* **2017**, *46*, 126–157.
[27] B. Aguila, Q. Sun, X. L. Wang, E. O'Rourke, A. M. Al-Enizi, A. Nafady, S. Q. Ma, *Angew. Chem. Int. Ed.* **2018**, *57*, 10107–10111.
[28] L. Feng, K. Y. Wang, G. S. Day, M. R. Ryder, H. C. Zhou, *Chem. Rev.* **2020**, *120*, 13087–13133.
[29] S. A. Burgess, A. Kassie, S. A. Baranowski, K. J. Fritzsching, K. Schmidt-Rohr, C. M. Brown, C. R. Wade, *J. Am. Chem. Soc.* **2016**, *138*, 1780–1783.
[30] J. S. Lee, E. A. Kapustin, X. K. Pei, S. Llopis, O. M. Yaghi, F. D. Toste, *Chem* **2020**, *6*, 142–152.
[31] J. K. Jin, K. Wu, X. Y. Liu, G. Q. Huang, Y. L. Huang, D. Luo, M. Xie, Y. F. Zhao, W. G. Lu, X. P. Zhou, J. He, D. Li, *J. Am. Chem. Soc.* **2021**, *143*, 21340–21349.
[32] X. L. Xu, N. N. Wang, Y. H. Zou, X. Qin, P. Wang, X. Y. Lu, X. Y. Zhang, W. Y. Sun, Y. Lu, *Nat. Commun.* **2024**, *15*, 7273.
[33] X. Chen, Y. W. Peng, X. Han, Y. Liu, X. C. Lin, Y. Cui, *Nat. Commun.* **2017**, *8* 2171.
[34] S. L. Hou, J. Dong, X. L. Jiang, Z. H. Jiao, B. Zhao, *Angew. Chem. Int. Ed.* **2019**, *58*, 577–581.
[35] L. Zhu, X. Q. Liu, H. L. Jiang, L. B. Sun, *Chem. Rev.* **2017**, *117*, 8129–8176.

[36] V. Pascanu, G. G. Miera, A. K. Inge, B. Martín-Matute, *J. Am. Chem. Soc.* **2019**, *141* 7223–7234.
[37] C. C. Cao, C. X. Chen, Z. W. Wei, Q. F. Qiu, N. X. Zhu, Y. Y. Xiong, J. J. Jiang, D. W. Wang, C. Y. Su, *J. Am. Chem. Soc.* **2019**, *141*, 2589–2593.
[38] C. Gao, J. Li, S. Yin, J. L. Sun, C. Wang, *J. Am. Chem. Soc.* **2020**, *142*, 3718–3723.
[39] Y. Jung, C. W. Lee, B. H. Lee, Y. Yu, J. Moon, H. S. Lee, W. Ko, J. Bok, K. Lee, J. Lee, M. S. Bootharaju, J. Ryu, M. Kim, T. Hyeon, *J. Am. Chem. Soc.* **2024**, *147*, 1740–1748, https://doi.org/10.1021/jacs.4c13057.
[40] J. Song, Z. Luo, D. K. Britt, H. Furukawa, O. M. Yaghi, K. I. Hardcastle, C. L. Hill, *J. Am. Chem. Soc.* **2011**, *133*, 16839–16846.
[41] M. Babucci, A. Guntida, B. C. Gates, *Chem. Rev.* **2020**, *120*, 11956–11985.
[42] A. Bavykina, N. Kolobov, I. S. Khan, J. A. Bau, A. Ramirez, J. Gascon, *Chem. Rev.* **2020**, *120*, 8468–8535.
[43] Y. S. Wei, M. Zhang, R. Q. Zou, Q. Xu, *Chem. Rev.* **2020**, *120*, 12089–12174.
[44] J. Guo, Y. T. Qin, Y. F. Zhu, X. F. Zhang, C. Long, M. T. Zhao, Z. Y. Tang, *Chem. Soc. Rev.* **2021**, *50*, 5366–5396.
[45] Z. Jiang, X. H. Xu, Y. H. Ma, H. S. Cho, D. Ding, C. Wang, J. Wu, P. Oleynikov, M. Jia, J. Cheng, Y. Zhou, O. Terasaki, T. Y. Peng, L. Zan, H. X. Deng, *Nature* **2021**, *590*, E16–E16.
[46] Y. J. Fan, A. L. Blenko, S. Labalme, W. B. Lin, *J. Am. Chem. Soc.* **2024**, *146*, 7936–7941.
[47] B. I. Z. Ahmad, R. T. Jerozal, S. J. Meng, C. Oh, Y. Cho, H. J. Kulik, T. H. Lambert, P. J. Milner, *J. Am. Chem. Soc.* **2024**, *146*, 34743–34752.
[48] K. Sun, Y. Huang, F. S. Sun, Q. Y. Wang, Y. J. Zhou, J. X. Wang, Q. Zhang, X. S. Zheng, F. T. Fan, Y. Luo, J. Jiang, H. L. Jiang, *Nat. Chem.* **2024**, *16*, 1638–1646.
[49] H. H. Hu, Z. Y. Wang, L. Y. Cao, L. Z. Zeng, C. K. Zhang, W. B. Lin, C. Wang, *Nat. Chem.* **2021**, *13*, 358–366.
[50] G. C. Guo, J. P. Zhao, S. Guo, W. X. Shi, F. C. Liu, T. B. Lu, Z. M. Zhang, *Angew. Chem., Int. Ed.* **2024**, *63*, e202402374.
[51] J. Guo, Q. Xia, W. Y. Tang, Z. K. Li, X. Wu, L. J. Liu, W. P. To, H. X. Shu, K. H. Low, P. C. Y. Chow, T. W. B. Lo, J. He, *Nat. Catal.* **2024**, *7*, 307–320.
[52] P. Kittikhunnatham, G. A. Leith, A. Mathur, J. K. Naglic, C. R. Martin, K. C. Park, K. McCullough, H. D. A. C. Jayaweera, R. E. Corkill, J. Lauterbach, S. G. Karakalos, M. D. Smith, S. Garashchuk, D. A. Chen, N. B. Shustova, *Angew. Chem. Int. Ed.* **2022**, *61*, e202113909.
[53] G. F. Ji, L. Zhao, J. W. Wei, J. K. Cai, C. He, Z. G. Du, W. Cai, C. Y. Duan, *Angew. Chem. Int. Ed.* **2022**, *61*, e202114490.
[54] A. Basak, S. Karak, R. Banerjee, *J. Am. Chem. Soc.* **2023**, *145*, 7592–7599.
[55] J. A. Johnson, B. M. Petersen, A. Kormos, E. Echeverría, Y. S. Chen, J. Zhang, *J. Am. Chem. Soc.* **2016**, *138*, 10293–10298.
[56] R.-R. Liang, Y. Fu, Z. Han, Y. Yang, V. I. Bakhmutov, Z. Liu, J. Rushlow, H.-C. Zhou, *Nat. Water* **2024**, *2*, 1218–1225.
[57] T. C. Wang, N. A. Vermeulen, I. S. Kim, A. B. F. Martinson, J. F. Stoddart, J. T. Hupp, O. K. Farha, *Nat. Protoc.* **2016**, *11*, 149–162.
[58] I. del Castillo-Velilla, A. Sousaraei, I. Romero-Muñiz, C. Castillo-Blas, A. S. J. Méndez, F. E. Oropeza, V. A. D. O'Shea, J. Cabanillas-González, A. Mavrandonakis, A. E. Platero-Prats, *Nat. Commun.* **2023**, *14*, 2506.
[59] J. X. Lin, J. Ouyang, T. Y. Liu, F. X. Li, H. H. Y. Sung, I. Williams, Y. J. Quan, *Nat. Commun.* **2023**, *14*, 7757.
[60] K. McRoberts, W. Z. Zhou, *CrystEngComm* **2021**, *23*, 7658–7662.
[61] C. Koschnick, R. Stäglich, T. Scholz, M. W. Terban, A. von Mankowski, G. Savasci, F. Binder, A. Schökel, M. Etter, J. Nuss, R. Siegel, L. S. Germann, C. Ochsenfeld, R. E. Dinnebier, J. Senker, B. V. Lotsch, *Nat. Commun.* **2021**, *12*, 3099.
[62] L. X. Hou, X. Jing, H. L. Huang, C. Y. Duan, *J. Mater. Chem. A* **2022**, *10*, 24320–24330.
[63] D. C. Mayer, A. Manzi, R. Medishetty, B. Winkler, C. Schneider, G. Kieslich, A. Pöthig, J. Feldmann, R. A. Fischer, *J. Am. Chem. Soc.* **2019**, *141*, 11594–11602.
[64] Y. Takeda, *Accounts. Chem. Res.* **2024**, *57*, 2219–2232.
[65] Z. J. Chen, Z. Thiam, A. Shkurenko, L. J. Weselinski, K. Adil, H. Jiang, D. Alezi, A. H. Assen, M. O'Keeffe, M. Eddaoudi, *J. Am. Chem. Soc.* **2019**, *141*, 20480–20489.
[66] F. Saraci, V. Quezada-Novoa, P. R. Donnarumma, A. J. Howarth, *Chem. Soc. Rev.* **2020**, *49*, 7949–7977.
[67] J. P. Vizuet, M. L. Mortensen, A. L. Lewis, M. A. Wunch, H. R. Firouzi, G. T. McCandless, K. J. Balkus, *J. Am. Chem. Soc.* **2021**, *143*, 17995–18000.
[68] Y. C. Luo, F. F. Tong, Y. X. Zhang, C. Y. He, X. G. Zhang, *J. Am. Chem. Soc.* **2021**, *143*, 13971–13979.
[69] H. F. Yang, C. Li, T. Liu, T. Fellowes, S. Y. Chong, L. Catalano, M. Bahri, W. W. Zhang, Y. J. Xu, L. J. Liu, W. Zhao, A. M. Gardner, R. Clowes, N. D. Browning, X. B. Li, A. J. Cowan, A. I. Cooper, *Nat. Nanotechnol.* **2023**, *18*, 307–315.
[70] Y. Y. Guo, C. S. Abeywickrama, D. Y. J. Huo, J. Kong, M. Tao, A. D. Xia, Y. Pang, Y. Wan, *J. Phys. Chem. C* **2020**, *124*, 8550–8560.
[71] A. U. Neelambra, C. Govind, T. T. Devassia, G. M. Somashekharappa, V. Karunakaran, *Phys. Chem. Chem. Phys.* **2019**, *21*, 11087–11102.
[72] C. Liu, N. Shen, R. Shang, *Nat. Commun.* **2022**, *13*, 354.
[73] S. X. Cheng, J. Ouyang, M. Q. Li, Y. X. Diao, J. C. Yao, F. X. Li, Y. F. Lee, H. H. Y. Sung, I. Williams, Z. T. Xu, Y. J. Quan, *Angew. Chem. Int. Ed.* **2023**, *62*, e202300993.
[74] X. M. Li, X. Wang, Y. D. Li, J. X. Xiao, Y. F. Du, *Org. Biomol. Chem.* **2022**, *20*, 4471–4495.
[75] W. Zhou, I. A. Dmitriev, P. Melchiorre, *J. Am. Chem. Soc.* **2023**, *145*, 25098–25102.

Manuscript received: May 24, 2025
Revised manuscript received: June 03, 2025
Accepted manuscript online: June 06, 2025
Version of record online: June 17, 2025